10.1007/s12541-010-0020-5

A Review of Adhesion and Friction Models for Gecko Feet

Jae-Seob Kwak[1] and Tae-Wan Kim[1,#]

1 School of Mechanical Engineering, Pukyong National University, San 100, Yongdang-dong, Nam-gu, Busan, South Korea, 608-739
Corresponding Author / E-mail: tw0826@pknu.ac.kr, TEL: +82-51-629-6142, FAX: +82-51-629-6126

KEYWORDS: Adhesion, Friction, Gecko Feet, Peeling

The attachment pads of geckos exhibit the most versatile and effective adhesive known in nature. Their fibrillar structure is the primary source of high adhesion and their hierarchical structure produces the adhesion enhancement by giving the gecko the adaptability to create a large real area of contact with surfaces. Although geckos are capable of producing large adhesive forces, they retain the ability to remove their feet from an attachment surface at will. Detachment is achieved by a peeling motion of the gecko's feet from a surface. During the last few years, many researches have been conducted to develop the theoretical models that explain the gecko to adhere and detach from surfaces at will, including micro/macroscopic gecko adhesion, friction and peeling models for gecko hierarchical fibrillar structure contacting to rough surface. This review describes the progress in the modeling filed for gecko adhesion, friction and peeling, and discussed the future issues for gecko modeling.

Manuscript received: February 25, 2009 / Accepted: November 3, 2009

1. Introduction

Since the discovery of the ability of the gecko to "run up and down a tree in any way, even with the head downwards" by Aristotle,[1] the attachment pads of geckos have been widely studied. Gecko adhesive pads consist of arrays of micro and nano-scale fibers, often angled and with branching hierarchical structures. The tips of these fibers have a spatula shape to increase the contact area with the adhering surface. These fibers bend and conform to the surface roughness of climbing surfaces, creating large contact areas from millions or billions of contact points. Their hierarchical attachment system consists of ridges called lamellae that are covered in microscale setae that branch off into nanoscale spatulae. Each structure plays an important role in adapting to surface roughness bringing the spatulae in close proximity with the mating surface. It has been shown that van der Waals force,[2,3] possibly in combination with capillary forces[4,5] are responsible for the resulting adhesion. Although capable of generating high adhesion forces, a gecko is able to detach from a surface at will - an ability known as smart adhesion. Detachment is achieved by a peeling motion of the gecko's feet from a surface. During walking a gecko is able to peel its foot from surfaces by changing the angle at which its setae contact a surface. Using these adhesive pads, geckos can efficiently climb on both smooth and rough surfaces with repeatable, controllable adhesion without degradation. It is essential that the adhesive pad provide both friction and adhesion simultaneously to facilitate climbing.

Although there are over 1000 species of geckos[6,7] that have attachment pads of varying morphology,[8] the Tokay gecko (*Gekko gecko*) has been the main focus of scientific research.[9,10] The Tokay gecko is the second largest gecko species, attaining respective lengths of approximately 0.3-0.4 m and 0.2-0.3 m for males and females. They have a distinctive blue or gray body with orange or red spots and can weigh up to 300 g.[11] These geckos have been the most widely investigated species of gecko due to the availability and size of these creatures.

Even though the adhesive ability of geckos has been known since the time of Aristotle, little was understood about this phenomenon until the late nineteenth century when microscopic hairs covering the toes of the gecko were first noted. The development of electron microscopy in the 1950's enabled scientists to view a complex hierarchical morphology that covers the skin on the gecko's toes. Over the past century and a half, scientific studies have been conducted to determine the factors that allow the gecko

to adhere and detach from surfaces at will, including surface structure:[8,10,12-17] the mechanisms of adhesion;[2-4,8,9,18-25] and adhesive strength.[2,4,9,10,17,26]

In this review, the progress in the modeling filed for gecko adhesion, friction and peeling is described. In section 2, the extraordinary hierarchical structure of gecko feet and the known properties of gecko adhesive such as the compatibility to rough surface are presented briefly. Next, we described the adhesion models in the section 3: adhesion force models for single spatula which are van der Waals force[2,17,27] and capillary force,[4,28] fibrillar structure models contacting a rough surface,[3,17,29-37] multilevel hierarchical adhesion structure models,[29,30,38] and adhesion map for optimization of biomimetic attachment system.[39-41] For the friction, the fibrillar structure friction model based on Coulomb' law[42] and the adhesional friction model[43-45] are described, and for the peeling, the tape peeling models such as Kendall peel model[26,46-48] and peel zone model[84] are described in the section 4. Finally, we discussed the issues pending for the future in the section 5.

2. Gecko Feet

2.1 Structure of Tokay Gecko Feet

The explanation for the adhesive properties of gecko feet can be found in the surface morphology of the skin on the toes of the gecko. The skin is comprised of a complex hierarchical structure of lamellae, setae, branches, and spatulae.[8] As shown in Figs. 1 and 2 and summarized in Table 1, the gecko consists of an intricate hierarchy of structures beginning with lamellae, soft ridges that are 1-2 mm in length[8] that are located on the attachment pads (toes) that compress easily so that contact can be made with rough bumpy surfaces. Tiny curved hairs known as setae extend from the lamellae with a density of approximately 14000 per square millimeter.[15] These setae are typically 30-130 μm in length and 5-10 μm in diameter[8,9,12,14] and composed primarily of β-keratin[13,49] with some α-keratin component.[50] At the end of each seta, 100 to 1000 spatulae[8,9] with a diameter of 0.1-0.2 μm[8] branch out and form the points of contact with the surface. The tips of the spatulae are approximately 0.2-0.3 μm in width,[8] 0.5 μm in length and 0.01 μm in thickness[47] and get their name from their resemblance to a spatula.

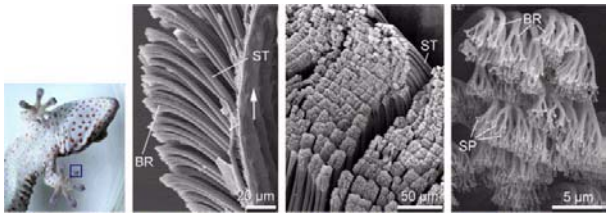

Fig. 1 The hierarchical structure of Tokay Gecko foot. ST, SP and BR represent seta, spatula and branch, respectively[32]

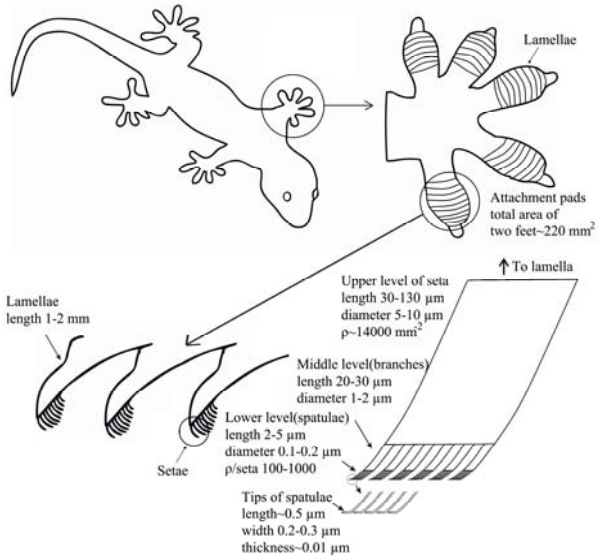

Fig. 2 Schematic drawings of a Tokay gecko including the overall body, one foot, a cross-sectional view of the lamellae and an individual seta. ρ represents number of spatulae[29]

Table 1 Surface characteristics of Tokay gecko feet (Young's modulus of surface material, keratin = 1-20 GPa)[13,56]

Component	Size	Density	F_{ad}
Seta	30-130[8,9,14] / 5-10[8,9,14] length/diameter (μm)	~14000[15,16] setae/mm^2	194 μN^2
Branch	20-30[8] / 1-2[8] length/diameter (μm)	-	-
Spatula	2-5[8] / 0.1-0.2[8,47] length/diameter (μm)	100-1000[8,9] spatulae/seta	-
Tip of spatula	~0.5[8,47] / 0.2-0.3[8,14] /~0.01[47] length/width/thickness (μm)	-	11 nN[26]

The attachment pads on two feet of the Tokay gecko have an area of about 220 mm^2. About three million setae on their toes can produce a clinging ability of about 20 N (vertical force required to pull a lizard down a nearly vertical (85°) surface)[10] and allow them to climb vertical surfaces at speeds of over 1 m/s with capability to attach or detach their toes in milliseconds. In isolated setae a 2.5 μN preload yielded adhesion of 20 to 40 μN and thus the adhesion coefficient, which represents the strength of adhesion as a function of preload ranges from 8 to 16.[3]

2.2 Compatibility to rough surface

Typical rough, rigid surfaces are only able to make intimate contact with a mating surface equal to a very small portion of the perceived apparent area of contact. In fact, the real area of contact is typically two to six orders of magnitude less than the apparent area of contact.[51,52] Autumn et al.[3] proposed that divided contacts serve as a means for increasing adhesion. A surface energy approach can be used to calculate adhesive force in the dry environment in order to calculate the effect of division on contacts. If the tip of a spatula is considered as a hemisphere with radius R_t adhesion force of a single contact F_{ad} based on the so called JKR (Johnson-Kendall-Roberts) theory,[53] is given as

$$F_{ad} = \frac{3}{2}\pi W_{ad} R_t \tag{1}$$

where W_{ad} is the work of adhesion (in units of energy per unit area). Eq. (1) shows that adhesive force of a single contact is proportional

to a linear dimension of the contact. For a constant area divided into a large number of contacts or setae, n, the radius of a divided contact R_d is given by $R_d = R_t/\sqrt{n}$ (self-similar scaling).[17] Therefore, the adhesive force of Eq. (1) can be modified for multiple contacts such that

$$F_{ad}^{'} = \frac{3}{2}\pi W_{ad}\left(\frac{R_t}{\sqrt{n}}\right)n = \sqrt{n}F_{ad} \tag{2}$$

where F'_{ad} is the total adhesive force from the divided contacts. Thus the total adhesion force is simply the adhesion force of a single contact multiplied by the square root of the number of contacts. For a contact in the humid environment, the meniscus (or capillary) forces further increase the adhesion force.[51,52,54] The attractive meniscus force, F_{m}, consists of a contribution by both Laplace pressure and surface tension.[54,55] Contribution by Laplace pressure is directly proportional to the meniscus area. The other contribution is from the vertical component of surface tension around the circumference. This force is proportional to the circumference as is the case for the work of adhesion.[51] Going through the analysis presented earlier, one can show that the contribution from the vertical component of surface tension increases with splitting into a larger number of contacts. It increases linearly with the square root of the number of contacts, n.[28]

$$(F_m')_{\text{ surface tension}} = \sqrt{n}(F_m)_{\text{ surface tension}} \tag{3}$$

where F_m' is the force from the divided contacts and F_m is the force of an individual contact. The models just presented only consider contact with a flat surface. On natural rough surfaces the compliance and adaptability of setae are the primary sources of high adhesion. Intuitively, the hierarchical structure of gecko setae allows for greater contact with a natural rough surface than non-branched attachment system.

Material properties also play an important role in adhesion. A soft material is able to achieve greater contact with a mating surface than a rigid material. Although gecko skin is comprised of β-keratin, a stiff material with a Young's modulus in the range of 1-20 GPa,[13,56] the effective modulus of the setal arrays on gecko feet is about 100 kPa,[57] which is approximately four orders of magnitude lower than the bulk material. The β-keratin material is relatively stiff to realize large contact area needed for high adhesion contact. Nature has selected a relatively stiff material to avoid clinging of adjacent setae. Division of contacts, as discussed earlier, provides high adhesion. By combining optimal surface structure and material properties, mother nature has created an evolutionary superadhesive.

3. Gecko Adhesion Models

When asperities of two solid surfaces are brought into contact with each other, chemical and/or physical attractions occur. The force developed that holds the two surfaces together is known as adhesion. In a broad sense, adhesion is considered to be either physical or chemical in nature.[27,51,52,54,58-61] Chemical interactions such as electrostatic attraction charges[20] as well as intermolecular forces[9] including van der Waals and capillary forces have all been proposed as potential adhesion mechanisms in gecko feet. Others have hypothesized that geckos adhere to surfaces through the secretion of sticky fluids,[18,19] suction,[19] increased frictional force,[21] and microinterlocking.[22] Through experimental testing and observations conducted over the last century and a half many potential adhesive mechanisms have been eliminated. Observation has shown that geckos lack glands capable of producing sticky fluids,[18,19] thus ruling out the secretion of sticky fluids as a potential adhesive mechanism. Furthermore, geckos are able to create large adhesive forces normal to a surface. Since friction only acts parallel to a surface, the attachment mechanism of increased frictional force has been ruled out. Dellit[22] experimentally ruled out suction and electrostatic attraction as potential adhesive mechanisms. Experiments carried out in vacuum did not show a difference between the adhesive forces at low pressures compared to ambient conditions. Since adhesive forces generated during suction are based on pressure differentials, which are insignificant under vacuum, suction was rejected as an adhesive mechanism.[22] Additional testing utilized X-ray bombardment to create ionized air in which electrostatic attraction charges would be eliminated. It was determined that geckos were still able to adhere to surfaces in these conditions and therefore, electrostatic charges could not be the sole cause of attraction.[22] Autumn et al.[2] demonstrated the ability of a gecko generate large adhesive forces when in contact with a molecularly smooth SiO_2 MEMS semiconductor. Since surface roughness is necessary for microinterlocking to occur, it has been ruled out as a mechanism of adhesion. Two mechanisms, van der Waals forces and capillary forces, remain as the potential sources of gecko adhesion.

Many adhesion models based on van der Waals force and capillary force, have been proposed to explain the gecko adhesion: adhesion force models for single spatula which are van der Waals force[2,17,27] and capillary force,[4,28] fibrillar structure models contacting a rough surface,[3,17,29-37] multilevel hierarchical adhesion structure models[29,30,38] and adhesion map for optimization of biomimetic attachment system.[39-41] These adhesion models are described in detail in the following sections.

3.1 Van der Waals Adhesion

Van der Waals bonds are secondary bonds that are weak in comparison to other physical bonds such as covalent, hydrogen, ionic, and metallic bonds. Unlike other physical bonds, van der Waals forces are always present regardless of separation and are effective from very large separations (~50 nm) down to atomic separation (~0.3 nm). The van der Waals force per unit area between two parallel surfaces, f_{vdW}, is given by[27,62,63]

$$f_{vdW} = \frac{A}{6\pi D^3}, \tag{4}$$

where A is the Hamaker constant and D is the separation between surfaces. Hiller[9] showed experimentally that the surface energy of a substrate is responsible for gecko adhesion. One potential adhesive mechanism would then be van der Waals forces.[2,24] Assuming van

der Waals forces to be the dominant adhesive mechanism utilized by geckos, the adhesive force of a gecko can be calculated. Typical values of the Hamaker constant range from 4×10^{-20} to 4×10^{-19} J.[27] In calculation, the Hamaker constant is assumed to be 10^{-19} J, the surface area of a spatula is taken to be 2×10^{-14} m^2,[8,14,16] and the separation between the spatula and contact surface is estimated to be 0.6 nm. This equation yields the force of a single spatula to be about 0.5 μN. By applying the surface characteristics of Table 1, the maximum adhesive force of a gecko is 150-1500 N for varying spatula density of 100-1000 spatulae per seta. If an average value of 550 spatulae/seta is used, the adhesive force of a single seta is approximately 270 μN which is in agreement with the experimental value obtained by Autumn et al..[2]

Another approach to calculate adhesive force is to assume that spatulae are cylinders that terminate in hemispherical tips. By using Eq. (1) and assuming that the radius of each spatula is about 100 nm and that the surface energy is expected to be 50 mJ/m^2,[17] the adhesive force of a single spatula is predicted to be 0.02 μN. This result is an order of magnitude lower than the first approach calculated for the higher value of A. For a lower value of 10^{-20} J for the Hamaker constant, the adhesive force of a single spatula is comparable to that obtained using the surface energy approach.

3.2 Capillary Adhesion Model

It has been hypothesized that capillary forces that arise from liquid mediated contact could be a contributing or even the dominant adhesive mechanism utilized by gecko spatulae.[9,24] Experimental adhesion measurements conducted on surfaces with different hydrophobicities and at various humidities[4] supports this hypothesis as a contributing mechanism. During contact, any liquid that wets or has a small contact angle on surfaces will condense from vapor in the form of an annular-shaped capillary condensate. Due to the natural humidity present in the air, water vapor will condense to liquid on the surface of bulk materials. During contact this will cause the formation of adhesive bridges (menisci) due to the proximity of the two surfaces and the affinity of the surfaces for condensing liquid.[64-65]

Kim and Bhushan[28] investigated the effects of capillarity on gecko adhesion by considering capillary force as well as the solid-to-solid interaction. The Laplace and surface tension components of the capillary force are treated as follows. Capillary force can be divided into two components: the Laplace force F_l and the surface tension force F_s such that the total capillary force F_c is given by the sum of the components

$$F_c = F_l + F_S, \tag{5}$$

The Laplace force is caused by the pressure difference across the interface of a curved liquid surface (Fig. 3) and depends on pressure difference multiplied by the meniscus area, which can be expressed as[55]

$$F_l = -\pi\kappa\gamma R_t^2 \sin^2\phi_f, \tag{6}$$

where γ is the surface tension, R_t is the tip radius, ϕ_f is the filling angle and κ is the mean curvature of meniscus. From the Kelvin equation[27] which is the thermal equilibrium relation, the mean curvature of meniscus can be determined as:

$$\frac{KT}{V\gamma}\ln\left(\frac{p}{p_o}\right) = \kappa \tag{7}$$

where K is the universal gas constant, T is the absolute temperature, V is the molecular volume, p_o is the saturated vapor pressure of the liquid at T, and p is the ambient pressure acting outside the curved surface(p / p_o is the relative humidity).

Orr et al.[55] formulated the mean curvature of meniscus between sphere and plane in terms of elliptical integrals. The filling angle ϕ_f can be calculated from the expression just mentioned and Eq. (7) using iteration method. Then the Laplace force is calculated for a given environment using Eq. (6). The surface tension of the liquid results in the formation of a curved liquid–air interface. The surface tension force acting on the sphere is

$$F_s = 2\pi R_t \gamma \sin\phi_f \sin(\theta_1 + \phi_f). \tag{8}$$

The surface tension force depends on radius. Therefore, division would result in an increase of the surface tension force by the square root of the number of contacts.[28] Hence, the total capillary force on the sphere is

$$F_c = \pi R_t \gamma \{2\sin\phi_f \sin(\theta_1 + \phi_f) - \kappa R_t \sin^2\phi_f\}. \tag{9}$$

For the solid-to-solid adhesion force, they used DMT theory[67] because Gecko's seta composed by β-keratin which has high elastic modulus is close to DMT model. The DMT adhesion force F_{DMT} between two round tips is calculated as

$$F_{DMT} = 2\pi R_t' W_{ad}, \tag{10}$$

where R'_t is the reduced radius of contact, which is calculated as $R'_t = 1/(R_{t1} + R_{t2})$; R_{t1}, R_{t2} – radii of contacting tips; for the case of similar tips, $R_t = R_{t1} = R_{t2}$, $R'_t = 2/R_t$. The work of adhesion W_{ad} can be calculated using the following equation for two flat surfaces separated by a distance D.[27]

$$W_{ad} = -\frac{A}{12\pi D^2}, \tag{11}$$

where A is the Hamaker constant which depends on the medium the two surfaces are in. Kim and Bhushan[28] assumed typical values of the Hamaker constant to be $A_a = 10^{-19}$ J in the air and $A_w = 6.7\times10^{-19}$ J in the water.[27] The work of adhesions of two surfaces in contact separated by an atomic distance $D \approx 0.2$ nm[27] are approximately

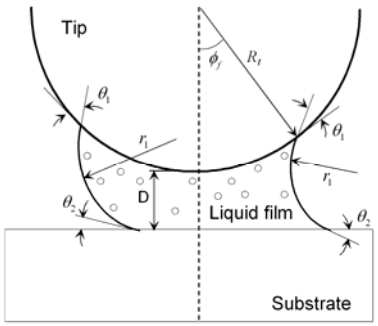

Fig. 3 Schematic of a sphere on a plane at distance D with a liquid film in between, forming menisci[28]

equal to 66 mJ/m^2 in the air and 44 mJ/m^2 in the water. Assuming tip radius R_t is 50 nm, the DMT adhesion forces of a single contact in the air and the water are $F_{DMT,a}$ =11 nN and $F_{DMT,w}$ =7.3 nN, respectively. As the humidity increases from zero to 100%, the DMT adhesion force will take a value between $F_{DMT,a}$ and $F_{DMT,w}$. To calculate the DMT adhesion force for the intermediate humidity, an approximation method by Wan et al.[68] is used. The work of adhesion W_{ad} for the intermediate humidity can be expressed as

$$W_{ad} = \int_D^\infty \frac{A}{6\pi h^3} dh = \int_D^{h_f} \frac{A_w}{6\pi h^3} dh + \int_{h_f}^\infty \frac{A_a}{6\pi h^3} dh \tag{12}$$

where h is the separation along the plane, h_f is the water film thickness at a filling angle ϕ_f, which can be calculated as

$$h_f = D + R_t(1-\cos\phi_f). \tag{13}$$

Therefore, using Eqs. (10), (12) and (13), the DMT adhesion force for the intermediate humidity gives as

$$F_{DMT} = F_{DMT,w}\left\{1 - \frac{1}{(1+R_t(1-\cos\phi_f)/D)^2}\right\} + \left\{\frac{F_{DMT,a}}{(1+R_t(1-\cos\phi_f)/D)^2}\right\} \tag{14}$$

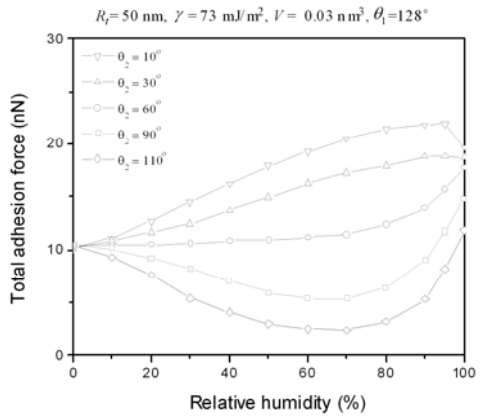

(a)

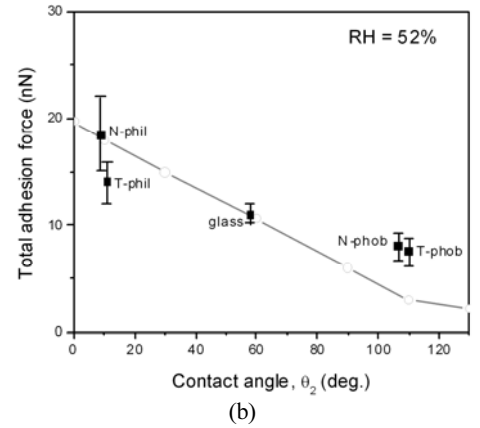

(b)

Fig. 4 (a) Total adhesion force as a function of relative humidity for a single spatula in contact with surfaces with different contact angles.[28] (b) Comparison the simulation results of Kim and Bhushan[28] with the measured data obtained by Huber et al.[4] for a single spatula in contact with the hydrophilic and the hydrophobic surfaces

Finally, Kim and Bhushan[28] calculated the total adhesion force F_{ad} as the sum of Eqs. (9) and (14):

$$F_{ad} = F_c + F_{DMT}. \tag{15}$$

To simulate the capillarity contribution to adhesion force for a gecko spatula, Kim and Bhushan[28] set the contact angle on gecko spatula tip θ_1 equal to 128°.[4] It was assumed that the spatula tip radius R_t = 50 nm, the ambient temperature T = 25°C, the surface tension of water γ = 73 mJ/m^2 and molecular volume of water V = 0.03 nm^3.[27]

Fig. 4(a) shows total adhesion force as a function of relative humidity for a single spatula in contact with surfaces with different contact angles. Total adhesion force decreases with an increase in the contact angle on the substrate, and the difference of total adhesion force among different contact angles is larger in the intermediate humidity regime. As the relative humidity increases, total adhesion force for the surfaces with contact angle less than 60° has higher value than the DMT adhesion force not considering wet contact, whereas with the value above 60°, total adhesion force has lower values at most relative humidities. The simulation results of Kim and Bhushan[28] are compared with the experimental data by Huber *et al.*[4] in Fig. 4(b). Huber *et al.*[4] measured the pull-off force of a single spatula in contact with four different types of Si wafer and glass at the ambient temperature 25°C and the relative humidity 52%. According to their description, wafer families 'N' and 'T' in Fig. 4(b) differ by the thickness of the top amorphous Si oxide layer. The 'Phil' type is the cleaned Si oxide surface which is hydrophilic with a water contact angle ≈ 10°, whereas the 'Phob' type is Si wafer covered with a hydrophobic monolayer causing water contact angle > 100°. The glass has water contact angle of 58°. Huber *et al.*[4] showed that the adhesion force of a gecko spatula rises significantly for substrates with increasing hydrophilicity (adhesion force increases by a factor of two as mating surfaces go from hydrophobic to hydrophilic). As shown in Fig. 4(b), the simulation results of Kim and Bhushan[28] closely match the experimental data of Huber *et al.*.[4]

3.3 Fibrillar structure models

The explanation for the adhesive properties of gecko feet can be found in the surface morphology With regard to the natural living conditions of the animals, the mechanics of gecko attachment can be separated into two parts: the mechanics of adhesion of a single contact with a flat surface, and an adaptation of a large number of spatulae to a natural, rough surface. For the single contact, we have covered in the sections 3.1 and 3.2. In this section, fibrillar structure models are described. The mechanics of adhesion between a fibrillar structure and a rough surface as it relates to the design of biomimetic structures has been a topic of investigation by many researchers.[3,7,17,29-36]

Federle[69] classified theoretical arguments to explain the increase of adhesion forces achieved by fibrillar structures into three types: fracture mechanics model, contact mechanics (force scaling) model and work of adhesion model, which are based on different assumptions and are not fully compatible with each other.

Fracture mechanics model implies that adhesion is maximized

when the size of adhesive contacts is smaller than the critical crack length. A crack will propagate in a block of material when the elastic energy released is greater than or equal to the increased energy released associated with new surfaces. As the energy invested to create new surfaces is linearly related to crack length *CL*, a crack propagates once its length exceeds a critical value given by the Griffith criterion[70]

$$CL \geq \frac{2\gamma E}{\pi\sigma^2}, \tag{16}$$

where σ is the applied stress, γ is the surface energy and *E* is the elastic modulus of the material. Similar concepts have been applied to the detachment of adhesive setae.[71-73] When the contact size is reduced to the range of critical crack length or smaller, the adhesive strength increases and may come close to the maximum theoretical strength of the interface. When seta tips are larger, setae can detach by peeling (crack propagation), and the forces are expected to scale with contact radius. Even for larger setae, however, the shape of the tips can be optimized by making them slightly concave so that the stress is uniformly distributed over the contact zone.[72] Under these conditions, the theoretical contact strength can be achieved, which is determined by the specific type of intermolecular interaction (for van der Waals forces ~ 20 MPa). However, small departures from the optimum shape in larger setae strongly reduce adhesion. Adhesion becomes flaw-insensitive when the contact size is smaller than the Griffith crack length.[72,73]

Contact mechanics models[13,17,48] predict adhesion forces to scale with length and not with area. This scaling relationship has given rise to the idea that adhesion can be increased by splitting up the contact zone into many subcontacts. The adhesion force of multiple contacts F_{ad} can be increased by dividing the contact into a large number (*n*) of small contacts. A greater number of smaller spatulae should thus increase overall adhesion. This concept has used to explain the correlation of setal density with body size, because larger animals with relatively less available surface area such as geckos require a more effective adhesive system per unit attachment area than smaller animals such as insects.[17,48] One inherent assumption of this force scaling argument is that the pull off stress is distributed uniformly over all the setae of a hairy pad. However, this assumption will not hold when hairy pads detach from the surface by peeling so that stresses are concentrated at the edge of the pad.[73]

The work of adhesion model suggests that adhesion increases due to the bending and stretching of setae and associated energy losses during detachment.[33,34] Similarly to the conclusion derived from the contact mechanics model,[17,48] work of adhesion model suggests that splitting up the contact into finer subcontacts can lead to increased adhesion. However, this model considers the oblique setae which give more compliant to surface and a much higher adhesion force. The adhesion of the work of adhesion model mainly depends on the energy needed to detach a single seta. The effective work of adhesion W* of a fibrillar structure is the product of the density of setae N_A (the number of setae per unit pad area) and the energy *U* needed to detach a single seta. Assuming that a seta sticking to the surface with the force F_0 is bent or stretched normal to the substrate by δ_{max} before detachment, its energy of detachment *U* is

$$U = \frac{F_0 \delta_{\max}}{2}. \tag{17}$$

Oblique fibers are displaced perpendicular to the surface[29,31,33,34] by

$$\delta_{\max} = \delta_{bending} \cos\theta + \delta_{compressive} \sin\theta = \frac{4l^3 F_0 \cos^2\theta}{3\pi R^4 E} + \frac{lF_0 \sin^2\theta}{\pi R^2 E} \tag{18}$$

Where *R* and *l* are the radius and length of the seta, respectively, and θ is the seta angle. Combination of Eqs. (17) and (18) gives

$$U = \frac{F_0^2 l}{2\pi R^2 E}\left[\frac{4l^2}{3R^2}\cos^2\theta + \sin^2\theta\right]. \tag{19}$$

If N_A is the maximum number of perpendicular fibers per unit area permitted by the self-matting condition, only a smaller density of $N'_A = N_A \sin\theta$ is possible for sloped fibers. The angle-dependent effective work of adhesion of the fiber array is then

$$W^*_\theta = UN'_A = \frac{F_0^2 N_A l}{2\pi R^2 E}\sin\theta\left[\frac{4l^2}{3R^2}\cos^2\theta + \sin^2\theta\right]. \tag{20}$$

Eq. (20) shows that adhesion is maximized for an intermediate angle θ_{max}. For setae with a large fiber aspect ratio ($l/2R$>20)), W'_θ scales with $\sin\theta\cos^2\theta$ and is maximum at θ_{max}=35°.

The influence of surface roughness on the adhesion in the biological systems has also been in the focus of scientists for a decade.[16,29-31,40,41,47,73-75] A benefit of fibrillar structures is its ability to make contact with and adhere to various surfaces with varying degrees of surface roughness due to the effective increase in surface compliance. Persson and Gorb[47] has quantified some important aspects about adhesion properties against rough surface and determined the work necessary to fail a fibrillar interface in the presence of roughness. He found that the work to fail a fibrillar contact array decreases with an increase in roughness height variation. Hui et al.[75] showed using a simple statistical treatment of a single-level fibrillar structure how compliance can compensate for roughness and length variability. They consider the mechanical model of a fibrillar surface with different height deviation to examine the effect of roughness. They showed normalized adhesion

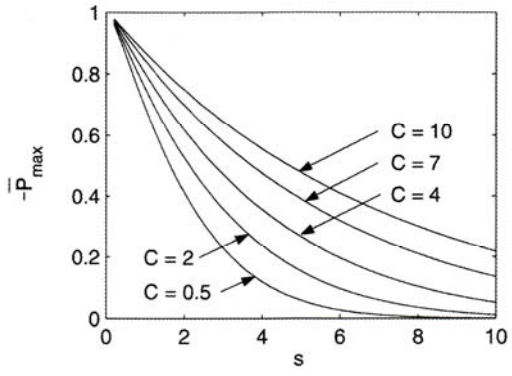

Fig. 5 Increasing surface roughness results in decreasing The variation of normalized adhesion strength, $-\bar{P}_{max}$ as a function of fibril height standard deviation, s. C represents fibrillar compliance[75]

strength, $-\bar{P}_{max}$ decreases with increasing fibril height standard deviation, s which represents roughness effect (Fig. 5). Kim and Bhushan[29,30] have recently approximated a gecko seta in contact with random rough surfaces using hierarchical spring model. They generated random rough surfaces by computer program,[51,52] and investigated the effect of surface roughness on the adhesion of fibrillar structure under a wide range of root mean square amplitude and various correlation lengths which are surface roughness parameters.

3.4 Multilevel hierarchical adhesion structure models

The explanation for the skin of gecko is comprised of a complex fibrillar structure of lamellae, setae, branches and spatulae.[8] The lamellae can adapt to the waviness of the surface while the setae and spatulae allow for the adaptation into micro and nanoroughness, respectively. Through the use of the hierarchical structure of its skin, gecko is able to bring a much larger percentage of its skin in contact with the mating surface. Intuitively, the hierarchical structure of gecko setae allows for a greater contact with a rough surface than a non-branched attachment system.[31] Several scientists have been trying to create hierarchical structure adhesive like gecko using various fabrication techniques.[76-80] However, there are few theoretical studies[29,30,38] on the effect of hierarchical structure on the adhesion enhancement.

In order to understand the effect of hierarchical adhesion structure on adhesion enhancements, the approach of Kim and Bhushan[29] will be described. They developed three-level hierarchical fibrillar structure model contacting a rough surface in terms of fracture mechanics, elastic beam theory and surface interaction forces. They simulated spring models with one, two and three levels of hierarchy to study the effect of the number of hierarchical levels in the attachment system on attachment ability

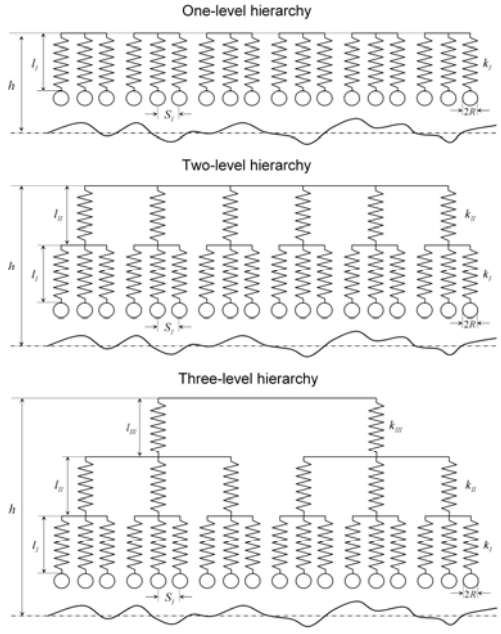

Fig. 6 One-, two- and three-level spring models for simulating the effect of hierarchical morphology on interaction of a seta with a rough surface[29]

(Fig. 6). Each level of springs in their model corresponds to a level of seta hierarchy. The upper level of springs corresponds to the thicker part of gecko seta, the middle spring level corresponds to the branches, and the lower level of springs corresponds to the spatulae. The upper level is the thickest branch of the seta. It is 75 μm in length and 5 μm in diameter. The middle level, referred to as a branch, has a length of 25 μm and diameter of 1 μm. The lower level, called a spatula, is the thinnest branch with a length of 2.5 μm and a diameter of about 0.1 μm. In their analysis, the tip of the spatula in a single contact is assumed as spherical. The springs on every level of hierarchy have the same stiffness as the bending stiffness of the corresponding branches of seta. From Eq. (18), the stiffness of seta branches k_m is calculated as

$$k_m = \frac{\pi R_m^2 E}{l_m \sin^2\theta(1+4l_m^2\cot^2\theta/(3R_m^2))}, \tag{21}$$

where subscript m is the level number. According to Derjaguin-Muller-Toporov (DMT) theory in Eq. (14), the adhesion force for a single tip of a spatula was calculated as 11 nN. This value is identical to the adhesion force of a single spatula measured by Huber et al..[26] This adhesion force is used as a critical force in the model for judging whether the contact between the tip and the surface is broken or not during pull off cycle.[38] If the elastic force of a single spring is less than the adhesion force, the spring is regarded as having been detached.

The base of the springs and the connecting plate between the levels are assumed to be rigid. The distance S_I between neighboring structures of level I was calculated as 0.35 μm and a 1:10 proportion of the number of springs in the upper level to that in the lower level was assumed.[29] The deflection of spring Δl was calculated as

$$\Delta l = h - l_0 - z, \tag{22}$$

where h is the position of the spring base relative to the mean line of surface; l_0 is the total length of a spring structure which is $l_0 = l_I$ for the one-level model, $l_0 = l_I + l_{II}$ for the two-level model, and $l_0 = l_I + l_{II} + l_{III}$ for the three-level model; and z is profile height of the rough surface. The elastic force F_{el} arisen in the springs at a distance h from the surface was calculated for the one-, two- and three- level models as[29]

$$F_{el} = -k_I \sum_{i=1}^{p} \Delta l_i u_i,\ u_i = \begin{cases} 1 & if\ contact \\ 0 & if\ no\ contact \end{cases} \tag{23}$$

$$F_{el} = -\sum_{j=1}^{q}\sum_{i=1}^{p} k_{ji}\left(\Delta l_{ji} - \Delta l_j\right) u_{ji},\ u_{ji} = \begin{cases} 1 & if\ contact \\ 0 & if\ no\ contact \end{cases}, \tag{24}$$

$$F_{el} = -\sum_{k=1}^{r}\sum_{j=1}^{q}\sum_{i=1}^{p} k_{kji}\left(\Delta l_{kji} - \Delta l_{kj} - \Delta l_j\right) u_{kji},\ u_{kji} = \begin{cases} 1 & if\ contact \\ 0 & if\ no\ contact \end{cases} \tag{25}$$

where p, q and r are the number of springs in the level I, II and III of the model respectively. When springs approach the rough surface, the spring force is calculated using either Eqs. (23), (24) and (25) for one-, two- and three-level models, respectively. During pull off, the same equations are used to calculate the spring force. However, when the applied load is equal to zero, the springs do not detach due

to adhesion attraction given by Eq. (10). Springs are pulled apart until the net force (pull-off force minus attractive adhesion force) at the interface is equal to zero. The adhesion force is the lowest value of elastic force F_{el} when the seta has detached from the contacting surface. The adhesion energy is calculated as

$$W_{ad} = \int_{\bar{D}}^{\infty} F_{el}(D)dD, \tag{26}$$

where D is the distance that the spring base moves away from the contacting surface. The lower limit of the distance $\bar{D}$ is the value of D where F_{el} is first zero when the model is pulled away from the contacting surface. The random rough surfaces used for simulation were generated by a computer program.[51,54] For modeling of contact of a seta with random rough surfaces, the range of values of σ from 0.01 μm to 30 μm and a fixed value of $\beta^* = 200$ μm were taken.

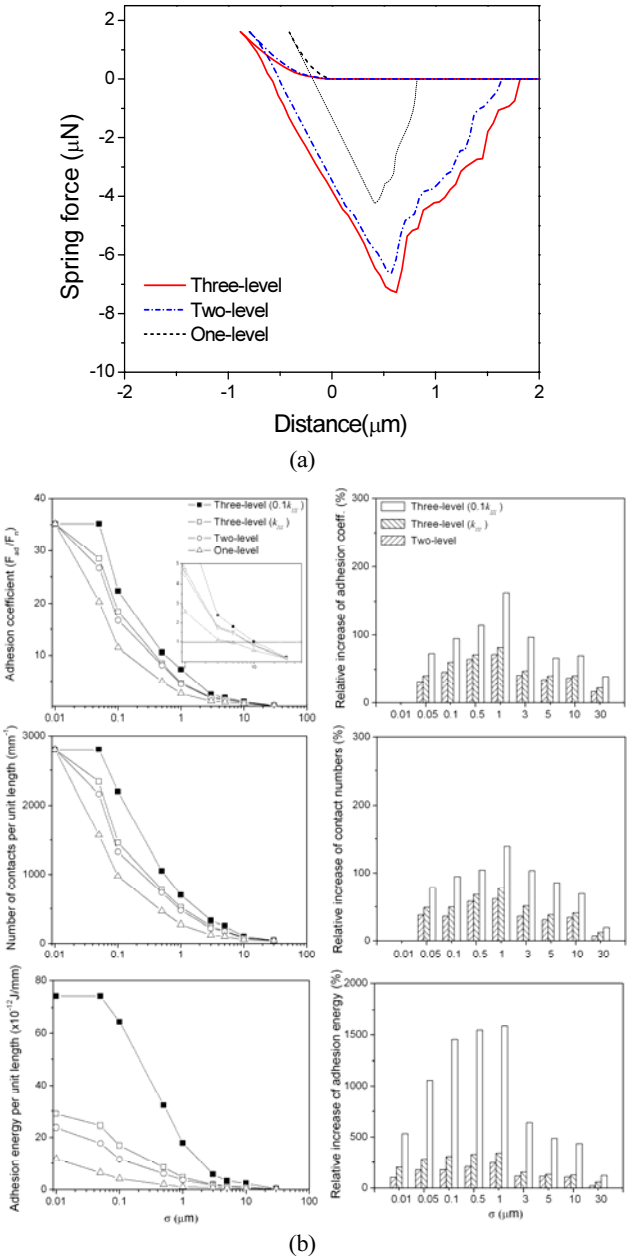

Fig. 7 (a) Force-distance curves of one-, two- and three-level models in contact with rough surfaces with σ = 1μm for an applied load of 1.6 μN.[29] (b) The adhesion coefficient, the number of contacts and the adhesion energy per unit length of profile for one- and multi-level models with an increase of σ value (left figures), and relative increases between multi- and one -level models (right side) for an applied load of 1.6 μN[29]

Fig. 7(a) shows the calculated spring force–distance curves for one-, two- and three-level hierarchical models in contact with rough surfaces with different values of root mean square (RMS) amplitude σ ranging from 0.01 μm to 10 μm at an applied load of 1.6 μN which was derived from the gecko's weight. Using the spring force-distance curves, Kim and Bhushan[29] calculated the adhesion coefficient, the number of contacts per unit length and the adhesion energy per unit length of the one-, two- and three-level models for an applied load of 1.6 μN and a wide range of RMS roughness as seen in the left graphs of Fig. 7(b). The adhesion coefficient, defined as the ratio of pull-off force to the applied preload, represents the strength of adhesion with respect to the preload. For the applied load of 1.6 μN, which corresponds to the weight of a gecko, the maximum adhesion coefficient is about 36 when σ is smaller than 0.01 μm. This means that a gecko can generate enough adhesion force to support 36 times its bodyweight. The adhesion coefficient decreases with an increase of σ. It is noteworthy that the adhesion coefficient falls below 1 when the contacting surface has an RMS roughness σ greater than 10 μm. This implies that the attachment system is no longer capable of supporting the gecko's weight. Autumn and coworkers[2,3] showed that in isolated gecko setae contacting with the surface of a single crystalline silicon wafer, a 2.5 μN preload yielded adhesion of 20–40 μN and thus a value of adhesion coefficient of 8–16, which supports the simulation results of Kim and Bhushan.[29] In order to demonstrate the effect of the hierarchical structure on adhesion enhancement, Kim and Bhushan[29] calculated the increases in the adhesion coefficient, the number of contacts, and the adhesion energy of the two-, three- and three-level (with $0.1k_{III}$) models relative to one-level model, as shown in the right side of Fig. 7(b). It was found for the two- and three-level models, relative increase of the adhesion coefficient increases slowly with an increase of σ and has the maximum values of about 70% and 80% at σ = 1 μm, respectively, and then decreases for surfaces with σ greater than 3 μm. Kim and Bhushan[29] did not consider the effect of lamellae in their study. The authors state that the lamellae can adapt to the waviness of surface while the setae allow for the adaptation to micro- or nano-roughness and expect that adding the lamellae of gecko skin to the model would lead to higher adhesion over a wider range of roughness.

3.5 Adhesion Map for Optimization of Biomimetic Attachment System

Effective design of geckolike adhesives requires deep understanding of the principle underlying the properties observed in the natural system. For example, synthetic setae that can attach without substantial preloads will likely require angled rather than vertical fibers to promote a bending rather than buckling mode of deformation.[31,81] It is necessary to ensure that the fibrils are compliant enough to easily deform to mating surface roughness

profile, yet rigid enough not to collapse. Excessively high dense setae should also cause matting of adjacent setae.[29-31,33,34,40,73] The distance between setae and the stiffness of the fibers will determine the amount of force required to bring the tips together for matting to occur. It follows form the cantilever model that stiffer, shorter and thicker stalks will allow a greater packing density without matting. Satisfying both non-sticking and rough surface conditions may require a compromise of design parameters. Shah and Sitti[39] studied using the fibers as an array of oriented cantilever beams mathematical relations between the adhesion properties and fiber properties, and formulated design guidelines for fabrication of the biomimetic synthetic adhesives. Spolenak et al.[40] devised design maps for setal adhesive structure, an elegant approach to visualizing the parametric trade-offs needed to satisfy the rough surface and non-sticking conditions. Kim and Bhushan[41] developed a convenient, general and useful guideline for understanding biological systems and for improving the biomimetic attachment. This adhesion database was constructed by modeling the fibers as oriented cylindrical cantilever beams with spherical tips. The authors then carried out numerical simulation of the attachment system in contact with random rough surfaces considering three constraint conditions—buckling, fracture and sticking of fiber structure. For a given applied load and roughness of contacting surface and fiber material, a procedure to find the optimal fiber radius and aspect ratio for the desired adhesion coefficient was developed.

4. Gecko Friction and Peeling Models

Although geckos are capable of producing large adhesive forces, they retain the ability to remove their feet from an attachment surface at will by peeling action. The orientation of the spatulae facilitates peeling. Autumn et al.[2] were the first to experimentally show that adhesive force of gecko setae is dependent on the three dimensional orientation as well as the preload applied during attachment. Due to this fact, geckos have developed a complex foot motion during walking. First the toes are carefully uncurled during attachment. The maximum adhesion occurs at an attachment angle of 30º—the angle between a seta and mating surface. The gecko is then able to peel its foot from surfaces one row of setae at a time by changing the angle at which its setae contact a surface. At an attachment angle greater than 30º the gecko will detach from the surface. This is consistent with models of setae a cantilever beams.[31,39,82] Gao et al.[32] created a finite element model of a single gecko seta in contact with a surface. A tensile force was applied to the seta at various angles, θ. They showed the dominant failure mode for forces applied at an angle less than 30° was sliding, whereas, the dominant failure mode for forces applied at angles greater than 30° was detachment. This verifies the results of Autumn et al.[2] that detachment occurs at attachment angles greater than 30º.

Several experimental reports[2,16,43,83] say that the friction force is higher than the adhesion force in the gecko adhesives. When properly oriented, preloaded and dragged, a single seta can generate 200 μN in shear[2] and 40 μN in adhesion,[16] over three orders of magnitude more than required to hold the animal's body weight. Autumn et al.[43] reported that when setal arrays dragged against their natural path (against curvature) they remained compressed and did not adhere. Average friction force F_f was 7.5 mN ± 0.00004, for an average normal (compressive) force, F_n of 25.0 ± 0.2 mN yielding a friction coefficient μ of 0.31±0.02. When dragged along their natural path (with curvature) setal arrays compressed initially and then adhered, resulting in tensile normal forces. Average friction force F_f in arrays dragged with curvature was 74.6 ± 9.0·mN and average normal force F_n (adhesion force F_{ad}) was 34.8 ± 4.6·mN. The angle of the resultant force vector was $\alpha^* = \tan^{-1}(F_n / F_f) = 24.6 \pm 0.9°$, which the detachment angle of the isolated seta arrays were close to the values of 30° in the past report.[2]

Several friction and peeling models have been proposed to explain the above experimental results for gecko hair's sliding and detachment. In this section, first, to explain the friction behavior on the fibrillar structure, the fibrillar structure friction model based on Coulomb' law[42] and the adhesional friction model[43-45] are described, and finally the tape peeling models such as Kendall peel model[26,40,46,47] and peel zone model[84] are demonstrated in detail in the following sections.

4.1 Friction in Fibrillar Structure

The friction force measured in the fibrillar structure is a combination of two types of forces: friction that is governed by Coulomb's law and adhesional friction. Coulomb's friction occurs when a fiber is in compression whereas adhesional friction is the lateral component of the tensile force on the fiber.

Majidi et al.[42] proposed a model for friction enhancement effect of fibrillar structure based on Coulomb's law. For a micro-rough substrate and/or small variations in fiber length, only a fraction of the fibers will be in contact under a small total normal load F_n. Fiber compliance can be modeled using either an ideal elastic column with a critical buckling load[37] or a inclined cantilever.[31] By Coulomb's law, shear resistance (friction force) of single fiber F'_t from each contact is

$$F_f^{'} = \mu F_{cr} + \tau A_f \tag{27}$$

where μ is friction coefficient, F_{cr} is critical buckling load of fiber, τ is the interfacial shear strength per unit area and A_f is the real contact area for the fiber. Under a light normal load F_n, it follows that for an array of ideal elastic columns, the number of contacts N will be approximately $N = F_n / F_{cr}$. With the addition of shear load, N should be slightly greater due to the enhanced compliance of fibers under compound loading, but this difference is assumed to be negligible.[42] The shear resistance of an entire fiber array F_f is as follows substituting the expressions for N and F'_t,

$$F_f = F_f^{'} N = \left(\mu + \frac{\tau A_f}{F_{cr}} \right) F_n = \mu_{eff} F_n \tag{28}$$

where μ_{eff} is the effective friction coefficient and Eq. (28) resembles Amontons' law. The ideal column model also implies complete

contact when the applied load exceeds $F_{cr}N_o$, where N_o is the total number of fibers inside the contact area. In this case,

$$\mu_{eff} = \mu + \frac{\tau N_o A_f}{F_n} \tag{29}$$

Since $N_o A_f$ is bounded above by the apparent contact area, Eq. (29) implies that μ_{eff} should asymptotically approach μ with increasing load F_n. Majidi et al.[42] measured the static friction on a traditional pulley apparatus for microfiber arrays from stiff polymer (polypropylene, 1GPa) as shown Fig. 8. The results show the fibrillar structure gives more than an order of magnitude increase in the friction coefficient compared to the bulk materials. As predicted in the above friction formulations for the fibrillar structure, the friction coefficients decrease with an increase of applied normal pressure as shown the fibers with radii of R = 0.3 μm and R = 0.6μm.

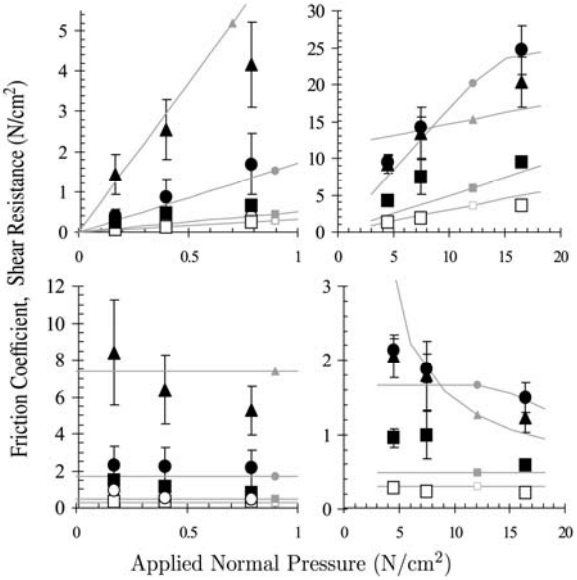

Fig. 8 Plot of shear resistance as a function of normal pressure for polypropylene fiber arrays; (▲) radius R = 0.3 μm, (●) R = 0.6 μm, (■) R = 2.5 μm. Solid gray lines represent theoretical predictions from Eq. (29)[42]

4.2 Frictional Adhesion Model

From several experiments,[2,16,43,83] it looks apparent that the friction forces are much higher than the adhesion forces. Autumn et al.[43] recently proposed a frictional adhesion model in which gecko adhesion depends directly on the shear (friction, lateral) force in the gripping direction. They also analyzed theoretically the gecko friction and adhesion behavior based on a tape model taking in to account the nano- and microscopic geometry and the macroscopic action of gecko toes.[44,45]

Tian et al's theoretical analysis[44] for frictional adhesion on microscale will be introduced. They used a tape model considering the final two levels of the hierarchical structures of geckos that are the seta and their spatulae as shown in Fig. 9. A seta has a length of approximately l_s = 120 μm, a cross-sectional diameter d_s = 4.2 μm. The spatula shaft has a diameter of approximately d =0.1 μm and a length of l = 0.8 μm. A spatula pad held at the end of a spatula shaft has approximate dimensions of 0.3 μm (length, L_p) × 0.2 μm (width, b) × 5 nm (thickness, h). The bending inertias of the seta shaft, spatula shaft and spatula pads are $I_s = 1.5 \times 10^{-23}$ m^4, $I' = 4.9 \times 10^{-30}$ m^4, and $I = 1.7 \times 10^{-32}$ m^4, respectively. They assumed the bulk elastic modulus E of the β keratin-like protein as 2 GPa.

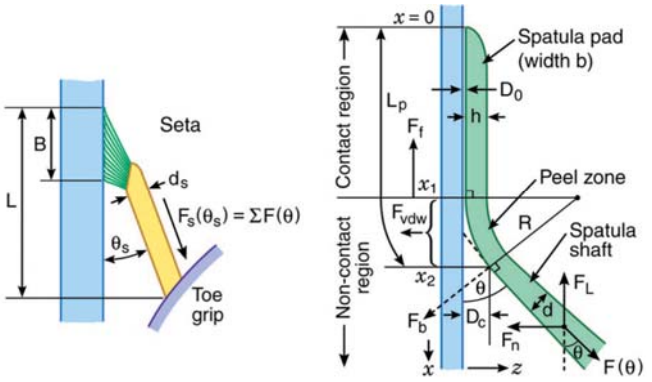

Fig. 9 A tape model for frictional adhesion on microscale considering the final two levels of the hierarchical structures of geckos that are the seta and their spatulae[44]

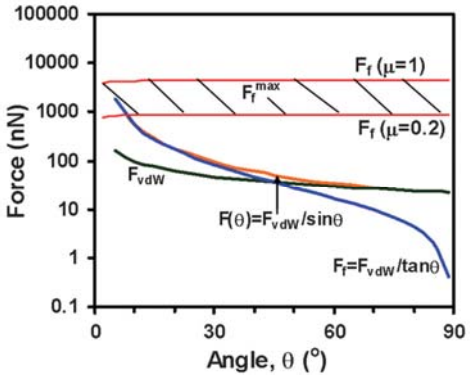

Fig. 10 The absolute values of the normal (adhesion) force component F_{vdW}, the lateral (friction) force component F_f, the net pulling force $F(\theta)$, and the maximum friction force F_f^{max} that can be obtained from a spatula pad in contact with a substrate (shaded band)[44]

The force balances in pulling a spatula analyzed in three force regime: (i) a contact region from x = 0 to $x = x_1$ where the attractive van der Waals force is balanced by the repulsive surface force, and where the total force on the spatula is therefore zero; (ii) a transition peel zone between x_1 and x_2 where the integrated van der Waals force F_{vdW} of the spatula is balanced by the force $F(\theta)$ along the spatula shaft; and (iii) for $x > x_2$, the van der Waals force acting on the shaft is too weak and is negligible, so the tension or pulling force remains constant and equal to $F(\theta)$ along the shaft. $F(\theta)$ can be written as

$$F(\theta) = F_n \sin\theta + F_L \cos\theta, \tag{30}$$

where the normal and lateral components F_n and F_L are defined as

$$F_n = F_{vdW} = F(\theta)\sin\theta \tag{31}$$

$$F_L = F_f = F(\theta)\cos\theta \tag{32}$$

For the radius of the spatula R, Tian et al. (2006) used an empirical power law of the form $R = 4.215\times\theta^{-1.35}$ for a physically realistic functional form for R in terms of θ that is valid at all angles. Based on this geometric relation, the attractive force in the peel zone F_{vdW} can be obtained by integrating the van der Waals force (Eq. (4)) from $\phi = 0$ to $\phi = \theta$, as follows

$$F_{vdw} = \int_0^{\theta}\left(\frac{A}{6\pi D^3}\right)bRd\phi = \int_0^{\theta}\left(\frac{A}{6\pi(D_0 + R(1-\cos\phi))^3}\right)bRd\phi, \quad (33)$$

where D_0 is the contact separation. Taking $A = 0.4\times10^{-19}$J and $D_0 =$ 0.3 nm, the curve of F_{vdW} are shown as a function of θ, which ranges from 20 nN at 90° to 150 nN at 5°. Tian et al. (2006) stated that instead of Eq. (33), the standard expression for the force between half a cylinder of radius R and a flat surface in following Eq. (34) gives almost the same results,

$$F_{vdW} = \frac{AbR^{1/2}}{16\sqrt{2}D^{5/2}}. \quad (34)$$

The attractive force in the contact regime ($x < x_1$) $F_{c,vdW}$ which determine the adhesion force contribution to the friction force F_f is

$$F_{c,vdW} = x_1 b\frac{A}{6\pi D_0^3}, \quad (35)$$

where $x_1 b$ is the contact area of a spatula with the substrate. The maximum friction force using the general equation for adhesion controlled is

$$F_f^{\max} = \mu F_{c,vdW}, \quad (36)$$

where μ is the friction coefficient. Because μ for a polymer material rubbing against a van der Waals surface usually ranges from 0.2 to 1.0, $F_f^{\max}$ is predicted to be ≈ 900–4,500 nN as shown in Fig. 10. The friction force of a single spatula has never been measured directly. Autumn *et al.* (2000) carried out a friction test on a single seta obtaining a maximum friction force of ≈ 200 μN. Taking the number of spatulae on a single seta to be 100–1,000, then $F_f^{\max}$ of a single spatula is 200–2,000 nN, which is in agreement with the above theoretical estimate.

The result graph of Tian et al.'s friction model (2006) is shown in Fig. 10. The friction force is $F_f = F_{vdW}/\tan\theta$, and the total pulling force is $F(\theta) = F_{vdW}/\sin\theta$. Fig. 10 shows the range of maximum possible values for $F(\theta)$ before the surfaces detach or slip. This regime, shown by the horizontal shaded band is determined mainly by $F_f^{\max}$. The condition $F(\theta) < F_f^{\max}$. is clearly satisfied for angles θ greater than ≈ 10°. Fig. 10 also shows that the pulling force $F(\theta)$ can vary by more than two orders of magnitude depending on θ and that for small θ ($\theta < 30°$) it is determined mainly by the friction force while for large θ ($\theta > 60°$) it is determined mainly by the adhesion force, the cross-over angle being at ≈ 40°. Tian et al.'s analysis[44] leads us to the comprehensive conclusion that both the lateral friction force and normal adhesion force of a single seta can be changed by more than three orders of magnitude.

4.3 Tape Peeling Model

A few studies[26,47,48] of the peeling of a single spatula have been analyzed in terms of the Kendall peeling model[46] as

$$\left(\frac{F}{b}\right)^2\frac{1}{2hE} + \left(\frac{F}{b}\right)(1-\cos\theta) - W_{ad} = 0, \quad (37)$$

where F is the peeling force, b is the width of the tape, h is the thickness of the tape, E is the elastic modulus of the tape and θ is the peeling angle. This equation, quadratic in F/b, shows how the three terms, elastic, potential and surface, interact. Ordinarily the first, elastic term may be neglected because the stress F/bh is usually very much smaller than E. The force during peeling of a flexible strip of tape including elastic energy term is given by

$$\frac{F}{b} = \frac{W_{ad}}{(1-\cos\theta)} + \ elastic\ energy\ term. \quad (38)$$

Solving for θ in Eq. (51), the angle at the onset of peeling is as

$$\theta = \cos^{-1}\left(1 - \frac{bW_{ad}}{F}\right). \quad (39)$$

The Kendall equation is derived based on an energy balance by considering the adhesive force between the tape and the surface and the amount of energy required to peel the tape to a new location while at a constant peel angle, θ. The Kendall equation inherently does not provide any information about the geometry of the peel zone nor how friction forces contribute to the adhesion force. To overcome this shortness, recently Pesika et al.[84] derived a new quantitative model for tape peeling based on the geometry of the peel zone, so called peel zone model, as ascertained form microscopic observations of the peel zone during detachment. Pesika et al.[84] derived the peeling force for the special case in which the tape backing is sufficiently compliant and the curvature of the backing.

$$\frac{F}{b} = \frac{2W_{ad}\theta}{\pi(1-\cos\theta)\sin\theta} \quad (40)$$

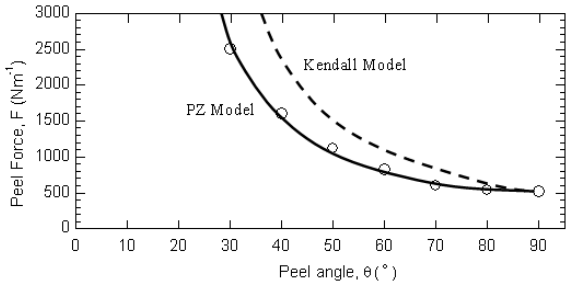

Fig. 11 Plots of measured and theoretical peel forces versus peel angle for a model tape consisting of a transfer tape adhesive on a transparency film backing at a peel velocity of $v \approx 0.03$ mm/s[84]

The PZ model derived Pesika et al.[84] differs from the Kendall equation (Eq. (38)) by an angle-dependent multiplier, which takes into account the increase in the length of the peel zone as the peel angle is reduced. This factor causes the peel force predicted by the peel zone model to be always smaller than the value given by the Kendall equation, the largest difference occurring at smaller peel angles. Fig. 11 shows a plot of the measured peel force for the detachment of the model tape from borosilicate glass surface as a

function of the peel angle θ in the range from 30° to 90°. The PZ model (solid line) accurately predicted the peeling behavior of the tape within the range of angles studied. The model accurately predicted the peel behavior for adhesive tapes. The Kendall model (dashed line) does predict the correct trend, but it increasingly overestimates the peel force as the peel angle decreases.

5. Future Works

In spite of many efforts in the gecko modeling field, they still fall short of the satisfying representation of gecko's performance. First, for the hierarchical models, there are many things to be developed. Kim and Bhushan[29] showed the roughness reduces the adhesion force; at the surface with σ more than 10 μm, adhesion force by gecko weight cannot support itself. However, in practice, gecko can cling or crawl on the surface of ceiling with higher roughness. Their model did not consider the effect of lamellae, soft ridge that are located on the attachment pads that compress easily so that contact can be made with rough bumpy surfaces. The lamellae can adapt to the waviness of surface while the setae allow for the adaptation to micro- or nano- roughness, so models of lamellar structure will be needed to explain function on roughness above the micron scale. In addition, the hierarchical models considered only normal to surface deformation and motion of seta. It should be noted that measurements of adhesion force of a single gecko seta made by Autumn et al.[2] demonstrated that a load applied normal to the surface was insufficient for an effective attachment of seta. The maximum adhesion force was observed by sliding the seta approximately 5 μm laterally along the surface under a preload. Therefore, the model for sliding and detachment motion of a hierarchical gecko structure needs to be considered. In addition, optimization for multi-level hierarchical adhesion system will be productive research topic.

Future work might also be aimed at establishing new interfacial laws to address the unique and remarkable properties of gecko feet. For the friction model, most of things are based on Coulomb's law, however there are many friction theories developed in the tribology area. Some more modern and sophisticated friction models can be applied to explain gecko sliding; adhesional friction models of elastomers,[85,86] ratchet models to present the effect of roughness on adhesional friction,[87-90] hysteresis models,[91,92] Liquid- mediated contact models.[93] Besides, the model to reveal the effect of surface roughness on the friction and peeling of gecko-like elastic thin films has not been discussed. The coupling model to explain the relationships between adhesion and friction is documented recently,[83] but more researches in the different respect need also to be presented. These theoretical works can motivate new insights into the friction and adhesion for fibrillar structures indeed.

Basic morphological description for biological diversity of lamellae, setae and spatulae will be required. Diversity of the array parameters, dimension and shape is great but not well documented. In particular, the shape for setal arrays on lamellae demands further investigation.[82] The collective behavior of the setal array will be a research topic.[72] The model on mechanical properties of a material like β keratin is also required for closer simulation to real.

One of the causes of the absence of the above models is the limitation of the experimental data. It is hard to study the mechanics of a single seta or a single spatula due to their small dimension. In particular, the separate contributions of the normal adhesion and lateral friction forces have not fully investigated. The rapid switching on and off of the adhesion and friction forces during a step involving attachment followed by detachment is still an open issue.[82] A possible reason is the oversimplification of the geometrical design of the artificial mimics. No hyperstrucrue, tilt, or optimized tip geometry has been considered. The main reason for the simplification is the intrinsic difficulty and scarce availability of 3D micro and nanofabrication methods for adhesion testing. This fact strongly limits further progress in this area.[80] Therefore, the greater experimental research efforts need to be encouraged.

The most immediate application of gecko inspired fibrillar structure is for wall climbing robots.[94-97] Stikybot which utilizes synthetic setal arrays for wall climbing is designed to achieve controllable adhesion through hierarchical structure compliance, anisotropic friction and adhesion, and distributed force control, similar the natural gecko.[97] Applications range from automobiles to electronic devices. Presently, manufacturers use glues, welding, or soldering to form temporary or weak permanent bonds. These methods consume material and time, require high precision, and often require multiple tools to execute. By replicating the characteristic of gecko feet adhesives, manufacturers hope to avoid these costly issues and enable the development of a super adhesive polymer tape capable of clean, dry adhesion.[31,76-78,98-106] High-friction microfiber arrays could also be used for enhanced traction in brakes and tiers. These reusable adhesives have potential for use in everyday objects such as tape, fasteners, and toys and in high technology such as microelectric and space applications. In addition, an issue for the potential utility of the developed modeling methods with Gecko inspired adhesive applications (e.g. how they can be used to design more effective adhesives) should be discussed delicately in the future.

In conclusion, the theoretical studies are contributing to understanding the fundamental processes underlying adhesion, friction and peeling, and providing biological inspiration for the design of novel adhesives and climbing robots.

ACKNOWLEDGEMENT

This work was supported by the Korea Research Foundation Grant funded by the Korean Government (MOEHRD, Basic Research Promotion Fund) (KRF-2008-331-D00051).

REFERENCES

1. Aristotle, "Historia Animalium," Trans. Thompson, D. A. W., 1918.

2. Autumn, K., Liang, Y. A., Hsieh, S. T., Zesch, W., Chan, W. P., Kenny, T. W., Fearing, R. and Full, R. J., "Adhesive force of a single gecko foot-hair," Nature, Vol. 405, No. 6787, pp. 681-685, 2000.

3. Autumn, K., Sitti, M., Liang, Y. A., Peattie, A. M., Hansen, W. R., Sponberg, S., Kenny, T. W., Fearing, R., Israelachvili, J. N. and Full, R. J., "Evidence for van der Waals adhesion in gecko setae," Proc. Natl. Acad. Sci. USA, Vol. 99, No. 19, pp. 12252-12256, 2002.

4. Huber, G., Mantz, H., Spolenak, R., Mecke, K., Jacobs, K., Gorb, S. N. and Arzt, E., "Evidence for capillarity contributions to gecko adhesion from single spatula and nanomechanical measurements," Proc. Natl. Acad. Sci. USA, Vol. 102, No. 45, pp. 16293-16296, 2005.

5. Sun, W., Neuzil, P., Kustandi, T. S., Oh, S. and Samper, V. D., "The nature of the gecko lizard adhesive force," Biophys. J. Vol. 89, No. 2, pp. 14-17, 2005.

6. Kluge, A. G., "Gekkotan lizard taxonomy," Hamadryad, Vol. 26, No. 1, pp. 1-209, 2001.

7. Han, D., Zhou, K. and Bauer, A. M., "Phylogenetic relationships among gekkotan lizards inferred from C-mos nuclear DNA sequences and a new classification of the Gekkota," Biol. J. Linn. Soc., Vol. 83, No. 3, pp. 353-368, 2004.

8. Ruibal, R. and Ernst, V., "The structure of the digital setae of lizards," J. Morph., Vol. 117, No. 3, pp. 271-294, 1965.

9. Hiller, U., "Untersuchungen zum Feinbau und zur Funktion der Haftborsten von Reptilien," Z. Morphol. Tiere., Vol. 62, No. 4, pp. 307-362, 1968.

10. Irschick, D. J., Austin, C. C., Petren, K., Fisher, R. N., Losos, J. B. and Ellers, O., "A comparative analysis of clinging ability among pad-bearing lizards," Biol. J. Linn. Soc., Vol. 59, No. 1, pp. 21-35, 1996.

11. Tinkle, D. W., "Gecko," Encylcopedia Americana, Grolier, Vol. 12, p. 359, 1992.

12. Russell, A. P., "A contribution to the functional morphology of the foot of the tokay, Gekko gecko," J. Zool. Lond., Vol. 176, No. 3, pp. 437-476, 1975.

13. Russell, A. P., "The morphological basis of weight-bearing in the scansors of the tokay gecko," Can. J. Zool., Vol. 64, No. 4, pp. 948-955, 1986.

14. Williams, E. E. and Peterson, J. A., "Convergent and alternative designs in the digital adhesive pads of scincid lizards," Science, Vol. 215, No. 4539, pp. 1509-1511, 1982.

15. Schleich, H. H. and Kästle, W., "Ultrastrukturen an Gecko-Zehen," Amphibia Reptilia, Vol. 7, No. 2, pp. 141-166, 1986.

16. Autumn, K. and Peattie, A. M., "Mechanisms of adhesion in geckos," Integr. Comp. Biol., Vol. 42, No. 6, pp. 1081-1090, 2002.

17. Arzt, E., Gorb, S. and Spolenak, R., "From micro to nano contacts in biological attachment devices," Proc. Natl. Acad. Sci. USA, Vol. 100, No. 19, pp. 10603-10606, 2003.

18. Wagler, J., "Naturliches System der Amphibien," J. G. Cotta'schen Buchhandlung, 1830.

19. Simmermacher, G.., "Untersuchungen uber haftapparate an tarsalgliedern von insekten," Zeitschr. Wiss. Zool., Vol. 40, No. 7, pp. 481-556, 1884.

20. Schmidt, H. R., "Zur Anatomie und Physiologie der Geckopfote," Jena. Z. Naturw., Vol. 39, No. 3, p. 551, 1904.

21. Hora, S. L., "The adhesive apparatus on the toes of certain geckos and tree frogs," J. Proc. Asiat. Soc. Beng., Vol. 9, No. 4, pp. 137-145, 1923.

22. Dellit, W. D., "Zur anatomie und physiologie der Geckozehe," Jena. Z. Naturw., Vol. 68, No. 3, pp. 613-658, 1934.

23. Gennaro, J. G. J., "The gecko grip," Nat. Hist., Vol. 78, No. 1, pp. 36-43, 1969.

24. Stork, N. E., "Experimental analysis of adhesion of Chrysolina polita on a variety of surfaces," J. Exp. Biol., Vol. 88, No. 1, pp. 91-107, 1980.

25. Bergmann, P. J. and Irschick, D. J., "Effects of temperature on maximum clinging ability in a diurnal gecko: evidence for a passive clinging mechanism?" J. Exp. Zool., Vol. 303A, No. 9, pp. 785-791, 2005.

26. Huber, G., Gorb, S. N., Spolenak, R. and Arzt, E., "Resolving the nanoscale adhesion of individual gecko spatulae by atomic force microscopy," Biol. Lett., Vol. 1, No. 1, pp. 2-4, 2005.

27. Israelachvili, J. N., "Intermolecular and Surface Forces: 2nd edition," Academic, 1992.

28. Kim, T. W. and Bhushan, B., "The adhesion model considering capillarity for gecko attachment system," J. Royal Soc. Interface, Vol. 5, No. 20, pp. 319-327, 2008.

29. Kim, T. W. and Bhushan, B., "Adhesion analysis of multi-level hierarchical attachment system contacting with rough surface," J. Adhesion Sci. Technol., Vol. 21, No. 1, pp. 1-20, 2007.

30. Kim, T. W. and Bhushan, B., "Effect of stiffness of multi-level hierarchical attachment system on adhesion enhancement," Ultramicroscopy, Vol. 107, No. 10-11, pp. 902-912, 2007.

31. Sitti, M. and Fearing, R. S., "Synthetic gecko foot-hair for micro/nano structures as dry adhesives," J. Adhesion Sci. Technol., Vol. 18, No. 8, pp. 1055-1074, 2003.

32. Gao, H., Wang, X., Yao, H., Gorb, S. and Arzt, E., "Mechanics of hierarchical adhesion structures of geckos," Mech. Mater., Vol. 37, No. 2-3, pp. 275-285, 2005.

33. Glassmaker, N. J., Jagota, A., Hui, C. Y. and Kim, J., "Design of biomimetic fibrillar interfaces: 1. Making contact," J. R. Soc. Interface, Vol. 1, No. 1, pp. 23-33, 2004.

34. Persson, B. N. J., "On the mechanism of adhesion in biological systems," J. Chem. Phys., Vol. 118, No. 16, pp. 7614-7621, 2003.

35. Glassmaker, N. J., Jagota, A. and Hui, C. Y., "Adhesion enhancement in a biomimetic fibrillar interface," Acta Biomaterialia, Vol. 1, No. 4, pp. 367-375, 2005.

36. Yao, H. and Gao, H., "Mechanics of robust and releasable adhesion in biology: bottom-up designed hierarchical structures of gecko," J. Mech. Phys. Solids, Vol. 54, No. 6, pp. 1120-1146, 2006.

37. Jagota, A. and Bennison, S. J., "Mechanics of adhesion through a fibrillar microstructure," Integr. Comp. Biol., Vol. 42, No. 6, pp. 1140-1145, 2002.

38. Bhushan, B., Peressadko, A. G. and Kim, T. W., "Adhesion analysis of two-level hierarchical morphology in natural attachment systems for 'smart adhesion'," J. Adhesion Sci. Technol., Vol. 20, No. 13, pp. 1475-1491, 2006.

39. Shah, G. J. and Sitti, M., "Modeling and design of biomimetic adhesives inspired by gecko foot-hairs," Proc. IEEE Int. Conf. on Robotics and Biomimetics, pp. 873-878, 2004.

40. Spolenak, R., Gorb, S. and Arzt, E., "Adhesion design maps for bio-inspired attachment systems," Acta Biomaterialia, Vol. 1, No. 1, pp. 5-13, 2005.

41. Kim, T. W. and Bhushan, B., "Optimization of Biomimetic Attachment System Contacting with a Rough Surface," J. Vac. Sci. Technol. A, Vol. 25, No. 4, pp. 1003-1012, 2007.

42. Majidi, C., Groff, R. E., Autumn, K., Baek, S., Bush, B., Gravish, N., Maboudian, R., Maeno, Y., Schubert, B., Wilkinson, M. and Fearing, R. S., "High friction from a stiff polymer using micro-fiber arrays," Phys. Rev. Lett., Vol. 97, No. 7, Paper No. 076103, 2006.

43. Autumn, K., Dittmore, A., Santos, D., Spenko, M. and Cutkosky, M., "Frictional Adhesion: a new angle on gecko attachment," J. Exp. Biol., Vol. 209, No. 18, pp. 3569-3579, 2006.

44. Tian, Y., Pesika, N. S., Zhao, B., Rosenberg, K., Zeng, H., McGuiggan, P., Autumn, K. and Israelachvili, J. N., "Adhesion and Friction in gecko toe attachment and detachment," Proc. Natl. Acad. Sci. USA, Vol. 103, No. 51, pp. 19320-19325, 2006.

45. Santos, D., Spenko, M., Parness, A., Kim, S. and Cutkosky, M., "Directional adhesion for climbing: theoretical and practical considerations," J. Adhesion Sci. Technol., Vol. 21, No. 12-13, pp. 1317-1341, 2007.

46. Kendall, K., "Thin-film peeling – the elastic term," J. Phys. D, Vol. 8, No. 13, pp. 1449-4452, 1975.

47. Persson, B. N. J. and Gorb, S., "The effect of surface roughness on the adhesion of elastic plates with application to biological systems," J. Chem. Phys., Vol. 119, No. 21, pp. 11437-11444, 2003.

48. Spolenak, R., Gorb, S., Gao, H. and Arzt, E., "Effects of contact shape on the scaling of biological attachments," Proc. R. Soc. Lond. A, Vol. 461, No. 2054, pp. 1-15, 2005.

49. Maderson, P. F. A., "Keratinized epidermal derivatives as an aid to climbing in gekkonid lizards," Nature, Vol. 203, pp. 780-781, 1964.

50. Rizzo, N., Gardner, K., Walls, D., Keiper-Hrynko, N. and Hallahan, D., "Characterization of the. structure and composition of gecko adhesive setae," J. Royal Soc. Interface, Vol. 3, No. 8, pp. 441-451, 2006.

51. Bhushan, B., "Introduction to Tribology," Wiley, pp. 154-156, 2002.

52. Bhushan, B., "Introduction to Nanotribology and Nano-mechanics," Springer-Verlag, pp. 354-368, 2005.

53. Johnson, K. L., Kendall, K. and Roberts, A. D., "Surface energy and the contact of elastic solids," Proc. R. Soc. Lond. A., Vol. 324, No. 1558, pp. 301-313, 1971.

54. Bhushan, B., "Principles and Applications of Tribology," Wiley, pp. 303-311, 1999.

55. Orr, F. M., Scriven, L. E. and Rivas, A. P., "Pendular rings between solids: meniscus properties and capillary force," J. Fluid Mech., Vol. 67, No. 4, pp. 723-742, 1975.

56. Bertram, J. E. A. and Gosline, J. M., "Functional design of horse hoof keratin: the modulation of mechanical properties through hydration effects," J. Exp. Biol., Vol. 130, No. 1, pp. 121-136, 1987.

57. Autumn, K., Majidi, C., Groff, R. E., Dittmore, A. and Fearing, R., "Effective elastic modulus of isolated gecko setal arrays," J. Exp. Biol., Vol. 209, No. 18, pp. 3558-3568, 2006.

58. Bikerman, J. J., "The Science of Adhesive Joints," Academic, 1961.

59. Zisman, W. A., "Influence of constitution on adhesion," Ind. Eng. Chem., Vol. 55, No. 10, pp. 18-38, 1963.

60. Houwink, R. and Salomon, G., "Effect of contamination on the adhesion of metallic couples in ultra high vacuum," J. Appl. Phys., Vol. 38, No. 4, pp. 1896-1904, 1967.

61. Bhushan, B., "Springer Handbook of Nanotechnology, 2nd Ed.," Springer-Verlag, pp. 605-624, 2006.

62. Hamaker, H. C., "London van der Waals attraction between spherical bodies," Physica, Vol. 4, No. 10, p. 1058, 1937.

63. Israelachvili, J. N. and Tabor, D., "The measurement of Van der Waals dispersion forces in the range of 1.5 to 130 nm," Proc. R. Soc. Lond. A, Vol. 331, No. 1584, pp. 19-38, 1972.

64. Zimon, A. D., "Adhesion of Dust and Powder, translated from Russian by M. Corn," Adhesion Science and Technology, 1969.

65. Fan, P. L. and O'Brien, M. J., "Adhesion in deformable isolated capillaries," Adhesion Science and Technology, 1975.

66. Phipps, P. B. and Rice, D. W., "Role of water in atmospheric corrosion," ACS Symposium Series, No. 89, 1979.

67. Derjaguin, B. V., Muller, V. M. and Toporov, Y. P., "Effect of contact deformation on the adhesion of particles," J. Colloid Interface Sci., Vol. 53, No. 2, pp. 314-326, 1975.

68. Wan, K. T., Smith, D. T. and Lawn, B. R., "Fracture and contact adhesion energies of mica-mica, silica-silica, and mica-silica interfaces in dry and moist atmospheres," J. Am. Ceram. Soc., Vol. 75, No. 3, pp. 667-676, 1992.

69. Federle, W., "Why so many adhesive pads hairy?" J. Exp. Biol., Vol. 209, No. 14, pp. 2611-2621, 2006.

70. Griffith, A. A., "The phenomena of rupture and flow in solids," Philos. Trans. R. Soc. Lond. A, Vol. 221, pp. 163-198, 1921.

71. Gao, H., Ji, B., Jaeger, I. L., Arzt, E. and Fratzl, P., "Materials become insensitive to flaws at nanoscale: lessons from nature," Proc. Natl. Acad. Sci. USA, Vol. 100, No. 10, pp. 5597-5600, 2003.

72. Gao, H. and Yao, H., "Shape insensitive optimal adhesion of nanoscale fibrillar structures," Proc. Natl. Acad. Sci. USA, Vol. 101, No. 21, pp. 7851-7856, 2004.

73. Hui, C. Y., Glassmaker, N. J., Tang, T. and Jagota, A., "Design of biomimetic fibrillar interfaces: 2. Mechanics of enhanced adhesion," J. R. Soc. Interface, Vol. 1, No. 1, pp. 35-48, 2004.

74. Huber, G., Gorb, S. N., Hosoda, N., Spolenak, R. and Arzt, E., "Influence of surface roughness on gecko adhesion," Acta Biomaterialia, Vol. 3, No. 4, pp. 607-610, 2007.

75. Hui, C. Y., Glassmaker, N. J. and Jagota, A., "How compliance compensates for surface roughness in fibrillar adhesion," J. Adhesion, Vol. 81, No. 7-8, pp. 699-721, 2005.

76. Northen, M. T. and Turner, K. L., "A batch fabricated biomimetic dry adhesive," Nanotechnology, Vol. 16, No. 8, pp. 1159-1166, 2005.

77. Northen, M. T. and Turner, K. L., "Meso-scale adhesion testing of integrated micro- and nano-scale structures," Sensors and Actuators A, Vol. 130-131, No. 8, pp. 583-587, 2006.

78. Sitti, M., "High aspect ratio polymer micro/nano-structure manufacturing using nanoembossing, nanomolding and directed self-assembly," Proc. IEEE/ASME Advanced Mechatronics Conf., Vol. 2, pp. 886-890, 2003.

79. Jeong, H. E., Lee, S. H., Kim, J. K. and Suh, K. Y., "Nanoengineered Multiscale Hierarchical Structures with Tailored Wetting Properties," Langmuir, Vol. 22, No. 4, pp. 1640-1645, 2006.

80. del Campo, A. and Arzt, E., "Design parameter and current fabrication approaches for developing bioinspired dry adhesives," Macromol. Biosci., Vol. 7, No. 2, pp. 118-127, 2007.

81. Aksak, B., Sitti, M., Casell, A., Li, J., Meyyappan, M. and Callen, P., "Friction of partially embedded vertically aligned carbon nanofibers inside elastomers," Appl. Phys. Lett., Vol. 91, No. 6, Paper No. 061906, 2007.

82. Autumn, K., "Properties, Principles, and Parameters of the Gecko Adhesive System," Biological Adhesives, pp. 225-256, 2006.

83. Zhao, B., Pesika, N. S., Tian, Y., Rosenberg, K., Zeng, H., McGuiggan, P., Autumn, K. and Israelachvili, J. N., "Adhesion and Friction force coupling of gecko setal arrays: Implications for structured adhesive surfaces," Langmuir, Vol. 24, No. 4, pp. 1517-1524, 2008.

84. Pesika, N., Tian, Y., Zhao, B., Rosenberg, K., Zeng, H., McGuiggan, P., Autumn, K. and Israelachvili, J. N., "Peel-zone model of tape peeling based on the gecko adhesive system," J. Adhesion, Vol. 83, No. 4, pp. 383-401, 2007.

85. Moore, D. F., "The friction and lubrication of Elastomers," Pergamon, 1972.

86. Bhushan, B., Sharma, B. S. and Bradshaw, R. L., "Friction in Magenetic Tapes I: Assessment of relevant theory," ASLE Trans., Vol. 27, No. 1, pp. 33-44, 1984.

87. Makinson, K. R., "On the cause of frictional difference of the wool fiber," Trans. Faraday Soc., Vol. 44, No. 2, pp. 279-282, 1948.

88. McFarlane, J. S. and Tabor, D., "Adhesion of solids and the effects of surface films," Proc. R. Soc. Lond. A., Vol. 202, No. 1069, pp. 224-243, 1950.

89. Tabor, D., "Adhesion and friction, in The Properties of Diamond," Academic, pp. 325-348, 1979.

90. Bhushan, B. and Ruan, J., "Atomic-scale friction measurements using friction force microscopy: Part II –

Application to magnetic media," ASME J. Tribol., Vol. 116, No. 3, pp. 452-458, 1994.

91. Tanaka, K., "Friction and deformation of polymers," J. Phys. Soc. Jpn., Vol. 16, No. 10, pp. 2003-2016, 1961.

92. Hegmon, R. R., "The contribution of deformation losses to rubber friction," Rubber Chem. and Technol., Vol. 42, No. 4, pp. 1122-1135, 1969.

93. Bhushan, B. and Zhao, Z., "Macro- and microscale tribological studies of molecularly-thick boundary layers of perfuluoropolyether Lubricants for magnetic thin-film rigid disks," J. Info. Storage proc. Syst., Vol. 1, No. 1, pp. 1-21, 1999.

94. Sitti, M. and Fearing, R. S., "Synthetic gecko foot-hair for micro/nano structures for future wall-climbing robots," Proc. IEEE Int. Conf. on Robotics and Automation, pp. 1164-1170, 2003.

95. Menon, C., Murphy, M. and Sitti, M., "Gecko inspired surface climbing robots," Proc. IEEE Int. Conf. on Robotics and Biomimetics, pp. 431-436, 2004.

96. Autumn, K., Buehler, M., Cutkosky, M., Fearing, R., Full, R. J., Goldman, D., Groff, R., Provancher, W., Rizzi, A. A., Sranli, U., Saunders, A. and Koditschek, D. E., "Robotics in scansorial environments," Proc. SPIE, Vol. 5804, pp. 291-302, 2005.

97. Kim, S., Spenko, M., Trujillo, S., Heyneman, B., Mattoli, V. and Cutkosky, M. R., "Whole body adhesion: hierarchical, directional and distributed control of adhesive forces for a climbing robot," Proc. IEEE Int. Conf. on Robotics and Automation, pp. 1268-1273, 2007.

98. Geim, A. K., Dubonos, S. V., Grigorieva, I. V., Novoselov, K. S., Zhukov, A. A. and Shapoval, S. Y., "Microfabricated adhesive mimicking gecko foot-hair," Nat. Mater., Vol. 2, No. 7, pp. 461-463, 2003.

99. Yurdumakan, B., Raravikar, N. R., Ajayan, P. M. and Dhinojwala, A., "Synthetic gecko foot-hairs from multiwalled carbon nanotubes," Chem. Comm., pp. 3799-3801, 2005.

100. Bhushan, B. and Sayer, R. A., "Surface characterization and friction of a bio-inspired reversible adhesive tape," Microsyst. Technol., Vol. 13, No. 1, pp. 71-78, 2007.

101. Burton, Z. and Bhushan, B., "Hydrophobicity, adhesion, and friction properties of nanopatterned polymers and scale dependence for micro- and nanoelectromechanical systems," Nano Letters, Vol. 5, No. 8, pp. 1607-1613, 2005.

102. Zhao, Y., Tong, T., Delzeit, L., Kashani, A., Meyyappan, M. and Majumdar, A., "Interfacial energy and strength of multiwalled-carbon-nanotube-based dry adhesive," J. Vac. Sci. Technol. B, Vol. 24, No. 1, pp. 331-335, 2006.

103. Kim, T. I., Jeong, H. E., Suh, K. Y. and Lee, H. H., "Stooped Nanohairs: Geometry-Controllable, Unidirectional, Reversible, Robust Gecko-like Dry Adhesive," Adv. Mater., Vol. 21, No. 22, pp. 2276-2281, 2009.

104. Jeong, H. E., Lee, J. K., Kim, H. N., Moon, S. H. and Suh, K. Y., "A nontransferring dry adhesive with hierarchical polymer nanohairs," Proc. Natl. Acad. Sci. USA, Vol. 106, No. 14, pp. 5639-5644, 2009.

105. Murphy, M. P., Kim, S. and Sitti, M, "Enhanced adhesion by gecko-inspired hierarchical fibrillar adhesives," ACS Appl. Mater. Interfaces, Vol. 1, No. 4, pp. 849-855, 2009.

106. Kobayashi, H., Moronuki, N. and Kaneko, A., "Self-assembly of Fine Particles Applied to the Production of Antireflective Surfaces," Int. J. Prec. Eng. Manuf., Vol. 9, No. 1, pp. 25-29, 2008.